SUPPORTING INFORMATION

β-Cyclodextrin Based Host–Guest Complexation of 3-(2-pyridyl) acrylic acid for Stability Enhancement and Aqueous-phase Ascorbic acid Detection.

Kangkan Mallick[a], Doli Roy[a], Priyanka Roy[a], Taniya Dey[b], Shilpi Ghosh[b], Subhankar Choudhury[c], Nitish Roy[a], Mahendra Nath Roy[a]*

[a]Department of Chemistry, University of North Bengal, Darjeeling 734013, India
[b]Department of Biotechnology, University of North Bengal, Darjeeling 734013, India
[c]Department of Chemistry, Malda College, Malda 732101, India
[a]*Corresponding Author, Mahendra Nath Roy, Department of Chemistry, NBU
*Corresponding Author E-mails:
mahendraroy2002@yahoo.co.in/mahendraroy2018@nbu.ac.in
Tel: +91-353-2776381, Fax: +91 353 2699001

Table of Contents

2.1 Materials: β-cyclodextrin (molecular weight = 1134.98 g.mol-1, purity > 99.0 %) was purchased by TCI Chemicals (India) and 3-(2-pyridyl) acrylic acid (molecular weight = 149.15 g.mol-1, purity > 98.0 %) was purchased by Sigma-Aldrich, India. Ascorbic acid, Glucose, Fructose, Citric acid, NaCl were bought from Alfa Aesar. Ethanol, acetone and other chemicals were bought from a local chemical company. All the chemicals were used without further modification, with all experiments carried out in double distilled water.

2.2 Instrumentation: The UV-vis absorption spectra were recorded using an Agilent 8453 spectrophotometer. Fluorescence spectra were measured with a Quantamaster-40 spectrofluorometer. The 1H NMR spectroscopic measurement were recorded on a Bruker neo 500 MHz spectrometer in DMSO solvent. FTIR (Fourier Transform Infrared Spectroscopy) spectra were recorded at ambient temperature by PerkinElmer 10.6.1 spectrometer instrument using KBr pellet method. The surface morphological analysis was performed using a scanning electron microscope (JSM-6360), It also examines the inclusion complex's morphological patterns and particle size. DSC analyses were performed on a Perkin Elmer DSC 6000 Instrument. The heating rate was 25 ◦C/min, going from 25 to 440 ◦C under a nitrogen atmosphere. TGA Q500 V20.13 Build 39 is used for Thermogravimetric analysis (TGA) samples using a in the temperature range of 30–600 °C with a heating rate of 10 °C per minute.

2.3. Antibacterial activity of the samples: The antibacterial activity of 3-PAA, β-CD-3-PAA and β-CD were assessed against two Gram-positive (Bacillus amyloliquifaciens and Staphylococcus aureus) and two Gram-negative bacteria (Klebsiella aerogenes and Escherichia coli). The qualitative antibacterial activities were checked by agar diffusion method [43], where 100 µl of freshly cultured (24 hr) Nutrient broth (NB) of the selected bacterial samples were spread on Nutrient agar (NA) plates and wells (5 mm diameter) were made using borer. Then 50 µl of the three testing samples (at a concentration of 1 mg/ml) along with DMSO as negative control were loaded onto the wells and incubated at 37 ℃ for 24 hours. After incubation the plates were checked for any growth inhibition zones around the wells and their diameters were measured.

The three testing samples were then checked for their minimal inhibitory concentrations (MIC) against the four bacterial strains. NB with varying concentrations (0.001, 0.002, 0.003, 0.004, 0.005, 0.007, 0.01, 0.03, 0.05, 0.07, 0.1, 0.3, 0.5, 1 mg/ml) of the samples were prepared and inoculated with 1% v/v 24-hour fresh NB cultures of the isolates and incubated at 37 ℃ for 24 hours, along with uninoculated NB as negative control. After incubation optical density at 600 nm of all the NBs were measured using spectrophotometry. The lowest concentrations with no visible bacterial growth (OD_{600} test $\leq$ OD_{600} control) were considered as the MIC of the samples.

2.4. Assessment of antioxidant activity

Antioxidant activity of PAA, β-CD-PAA and βCD were assessed using the following antioxidant assays:

1. ABTS+ radical scavenging assay: The spectrophotometric analysis of ABTS+ [2,2′-Azino-bis (3-ethylbenzothiazoline-6-sulfonic acid)] radical scavenging was achieved using the method described by Roy et al. (2023) [44]. The three testing samples in different concentrations were added to ABTS+ solution at 1:2 ratio and after 30 min of incubation in dark, their absorbance was recorded at 734 nm. The inhibition percentage was determined using the same formula as stated above.

2. DPPH radical scavenging assay: The in vitro scavenging of DPPH (2,2-diphenyl-1-picrylhydrazyl) radical was assessed following the method used by Haydar et al. (2022) [45]. The testing samples in different concentrations were mixed with 100 mM DPPH solution at 1:9 ratio and after 30 min of incubation in dark their absorbance was measured at 517 nm.

3. Superoxide scavenging assay: Superoxide radical scavenging assay was performed following the methodology used by Ghosh et al. (2023) [46]. Testing samples (1 ml) in different concentrations were mixed with 312 µM NBT solution (1 ml), 936 µM NADH (1 ml) solution and 120 µM PMS solution (10 µL); and after photo-induced reaction (using fluorescent light) their absorbance was recorded at 560 nm.

For all three assays reagents mixed with solvent (in same ratio as test samples) was taken as negative control and the inhibition percentage was calculated using the following equation.

$$\%\, Inhibition = \frac{A_c - A_s}{A_c} \times 100$$

Where, As = absorbance of the test sample and Ac = absorbance of the control. The IC50 values were determined using linear interpolation method (Alexander et al., 1999) [47].

2.5. Correlation of ^{1}H NMR Analysis with DFT-Optimized Geometry: To elucidate the inclusion orientation of 3-PAA within the β-CD cavity, the ^{1}H NMR chemical shift variations were systematically correlated with the DFT-optimized host–guest structure. Upon complex formation, the inner cavity protons of β-CD exhibited noticeable upfield shifts, with Δδ H3 = –0.0533 ppm and Δδ H5 = –0.1909 ppm (Table 1). Since H3 and H5 protons are located inside the hydrophobic cavity of β-CD, their shielding behavior directly reflects guest penetration depth. The significantly larger upfield shift observed for H5, which resides deeper within the cavity, indicates substantial insertion of the aromatic pyridine moiety into the inner hydrophobic

region. The greater magnitude of Δδ_H5 relative to Δδ_H3 suggests that 3-PAA preferentially enters from the wider rim of β-CD and extends toward the narrower rim, resulting in deep encapsulation of the aromatic segment (Fig.S1, Fig.S2c). This spectroscopic observation is in excellent agreement with the DFT-optimized geometry, which shows the pyridine ring embedded within the hydrophobic cavity while the carboxylic acid group remains near the rim region. The optimized structure further reveals hydrogen bonding interactions between the –COOH group of 3-PAA and the hydroxyl groups of β-CD, contributing to stabilization of the complex. The calculated binding constant (K_a = 1571.54 M^{-1}) supports the thermodynamic feasibility of this configuration.

The strong consistency between the experimentally observed NMR shielding pattern and the theoretical structural model confirms the proposed inclusion orientation and provides a comprehensive understanding of the supramolecular stabilization mechanism.

Table S1: Data for the Job plot performed by UV-visible spectroscopy for aqueous 3-PAA-β-CD system at 298.15 K[a]

3-PAA + β - CD							
3-PAA (mL)	**β-CD (mL)**	**3-PAA (μM)**	**β-CD (μM)**	**[3-PAA]/([3-PAA]+[β-CD])**	**Absorbance (A)**	**ΔA**	**[3-PAA]/([3-PAA]+[β-CD])**
0	3	0	100	0	0.0000	0.7980	0.0000
0.3	2.7	10	90	0.1	0.0520	0.7460	0.0746
0.6	2.4	20	80	0.2	0.1300	0.6680	0.1336
0.9	2.1	30	70	0.3	0.2080	0.5900	0.1770
1.2	1.8	40	60	0.4	0.3110	0.4870	0.1948
1.5	1.5	50	50	0.5	0.3650	0.4330	0.2165
1.8	1.2	60	40	0.6	0.4800	0.3180	0.1908
2.1	0.9	70	30	0.7	0.5670	0.2310	0.1617
2.4	0.6	80	20	0.8	0.6450	0.1530	0.1224
2.7	0.3	90	10	0.9	0.6940	0.1040	0.0936
3	0	100	0	1	0.7980	0.0000	0.0000

[a]Standard uncertainties in temperature T are u (T) = ± 0.01 K.

Table S2: Data for the Benesi-Hildebrand double reciprocal plot performed by UV-Vis spectroscopy for aqueous 3-PAA-β-CD system at 298.15 K[a].

[3-PAA] μM	**[β-CD]/μM**	**A_0**	**A**	**ΔA**	**1/[β-CD]**	**1/ΔA**	**Intercept**	**Slope**	**K_a/M^{-1}**
25	20	0.513	0.495	0.018	50000	55.55	1.7287	0.0011	1571.54
	40	0.513	0.477	0.036	25000	27.77			
	60	0.513	0.459	0.054	16666.6	18.51			
	80	0.513	0.443	0.07	12500	14.28			
	100	0.513	0.436	0.077	10000	12.98			
	120	0.513	0.429	0.084	8333.3	11.90			

[a]Standard uncertainties in temperature T are u (T) = ± 0.01 K.

Table S3: Blank Fluorescence dataset (n = 10)

Measurement	Blank Fluorescence (F0)
1	410612
2	410531
3	410598
4	410564
5	410625
6	410552
7	410587
8	410566
9	410602
10	410548

Table S4: LOD/LOQ calculation summary

Parameters	Value
Blank σ (n = 10)	63
Slope (ΔF vs AA)	1133
LOD (3σ/S)	0.18 μM
LOQ (10σ/S)	0.56 μM
R^2	> 0.99

Table S5. Effect of pH on fluorescence intensity and AA quenching efficiency of β-CD–3-PAA. The emission was monitored at 311 nm over the pH range 2.0–8.0.

pH	F_0 (a.u.)	F (with 80 µM AA)	ΔF	Quenching Efficiency (%)
2.0	358,200	139,700	218,500	61
3.0	396,800	111,700	285,100	72
4.0	410,500	102,400	308,100	75
5.0	418,200	99,900	318,300	76
6.0	415,600	108,900	306,700	74
7.0	402,400	112,600	289,800	72
8.0	370,200	129,600	240,600	65

[Quenching efficiency (%) = $(F_0 - F) / F_0 \times 100$]

Table S6: Fluorescence data and calculated ascorbic acid (AA) concentrations for real sample analysis using the β-CD–3-PAA IC-based fluorescence sensor (n = 3)

Sample	Added AA((µM)	F_0 (a.u.)	F (a.u.)	ΔF (F_0–F)	Calculated AA (µM)	Recovery (%)
Orange juice	40	410,200	371800	38,400	38.7	96.8
	80	410,200	333,100	77,100	82.1	102.4
Lemon juice	40	409,850	371,200	38,650	38.9	97.3
	80	409,850	332,400	77,450	81.6	102.0
Amla juice	40	411,300	369,900	41,400	41.2	103.1
	80	411,300	334,800	76,500	78.9	98.6
Guava juice	40	410,600	371,100	39,500	39.5	98.8
	80	410,600	331,900	78,700	82.7	103.4
Limcee tablet	—	412,000	—	—	496.3 mg	99.3

Table S7: **Bacterial growth inhibition zones by the samples**.

Zone of inhibition (in mm)				
	Bacillus amyloliquifaciens	*Staphylococcus aureus*	*Klebsiella aerogenes*	*Escherichia coli*
DMSO Control	0	0	0	0
3-PAA	15.33 ± 0.33	17.33 ± 0.33	20.33 ± 0.33	16.33 ± 0.33
β-CD-3-PAA	20.17 ± 0.17	24.67 ± 0.67	28.33 ± 0.33	25.17 ± 0.17
β-CD	15.83 ± 0.17	28.33 ± 0.33	21 ± 0.58	18.33 ± 0.33

Table S8: Minimum inhibitory concentration (MIC) of the samples.

MIC_{100} (mg/ml)			
	3-PAA	β-CD-3-PAA	β-CD
Bacillus amyloliquifaciens	0.3	0.005	0.07
Staphylococcus aureus	0.1	0.004	0.05
Klebsiella aerogenes	0.07	0.003	0.03
Escherichia coli	0.07	0.003	0.03

FIGURES

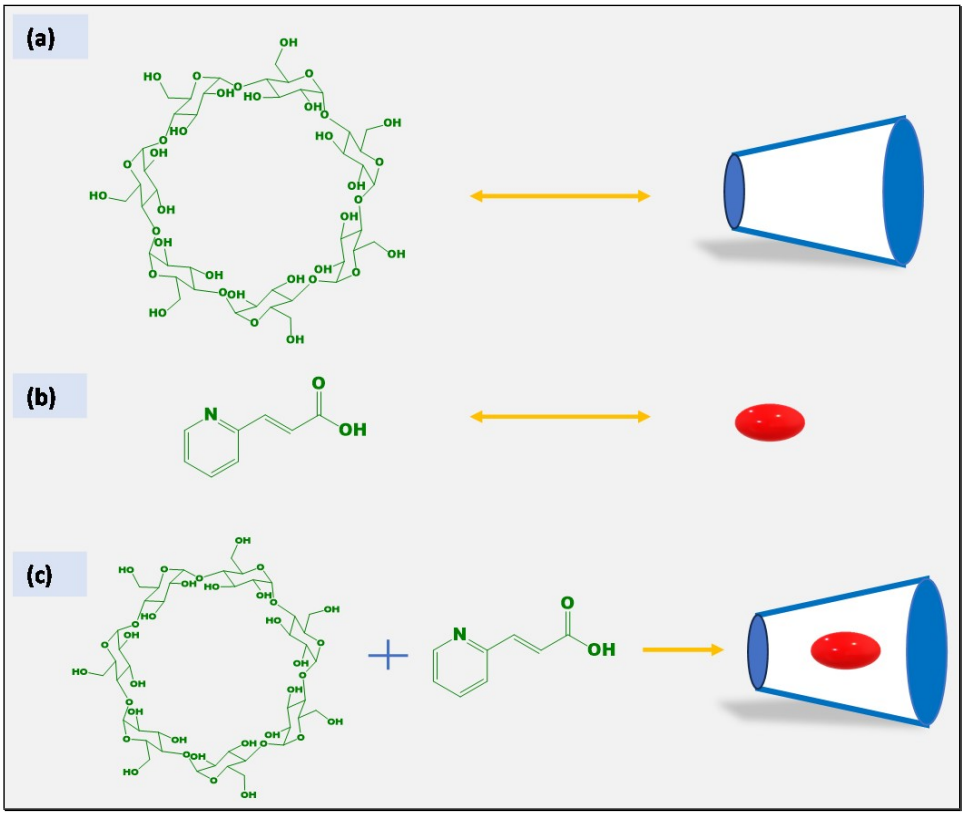

Fig.S1: (a) Molecular structure and schematic diagram of β-CD; (b) Molecular structure and schematic diagram of 3-PAA; (c) Molecular structure and schematic diagram of IC (3-PAA-β-CD).

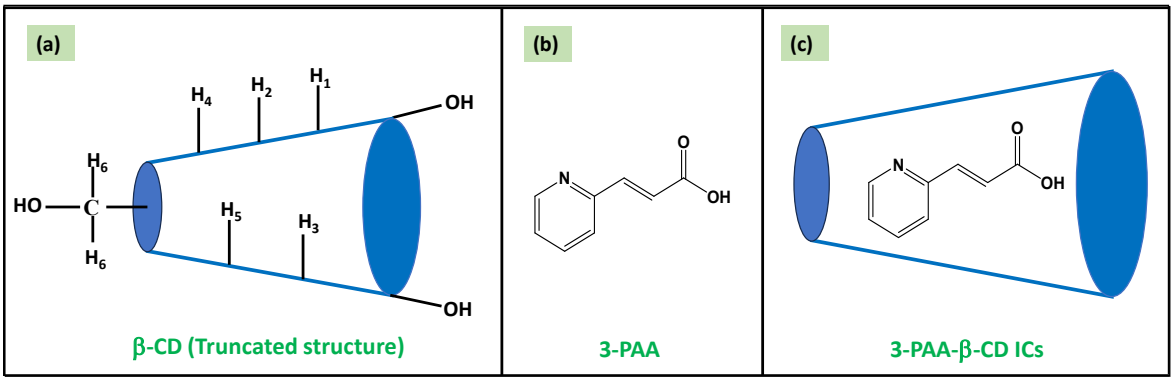

Fig.S2: Structure of (a) host (β-cyclodextrin), (b). guest (3-(2-pyridyl) acrylic acid), and (c) their inclusion complex.

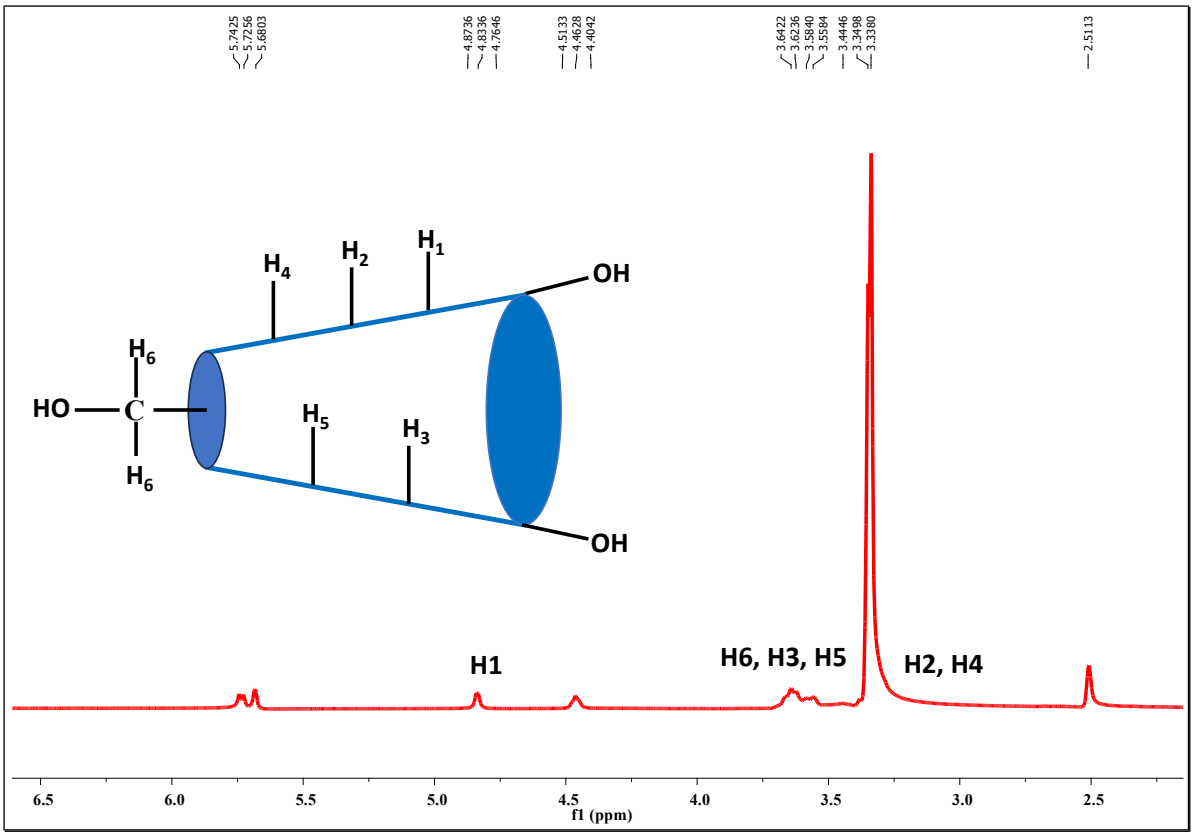

Fig.S3: ^{1}H NMR data of β-CD.

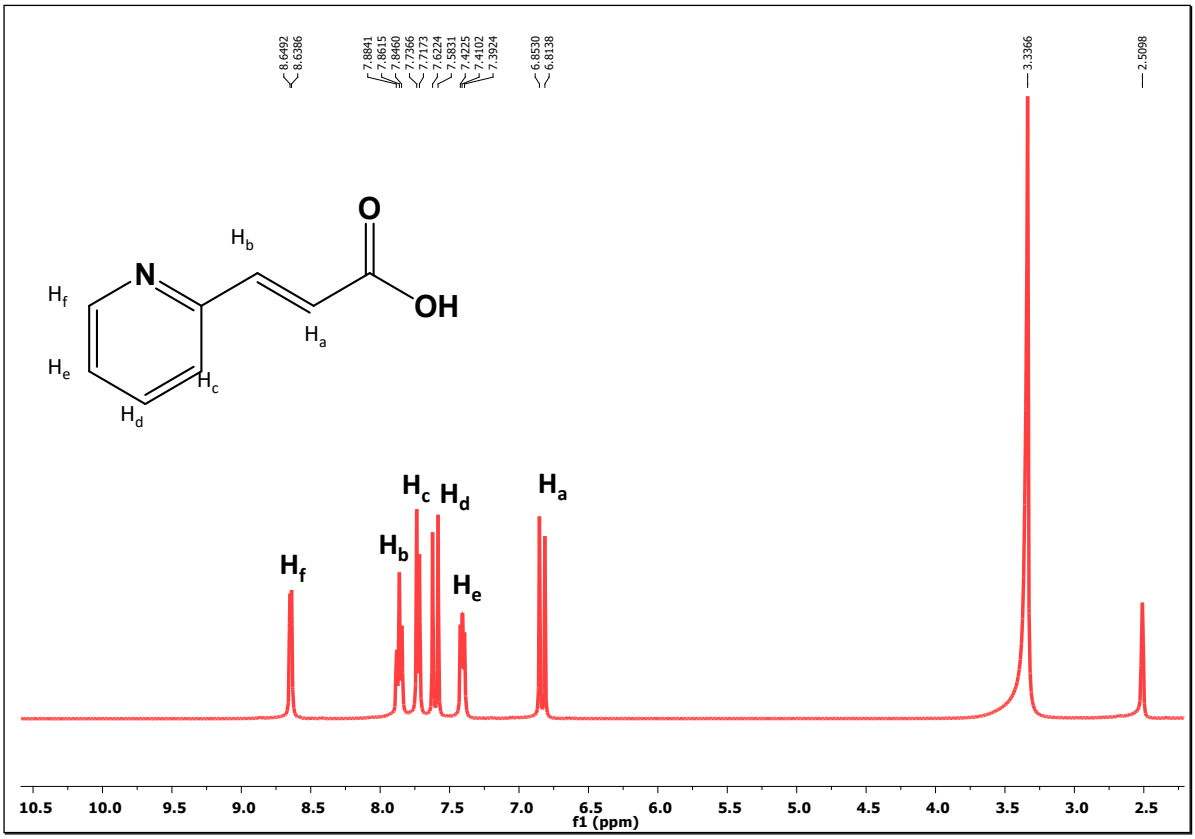

Fig.S4: ^{1}H NMR data of 3-PAA.

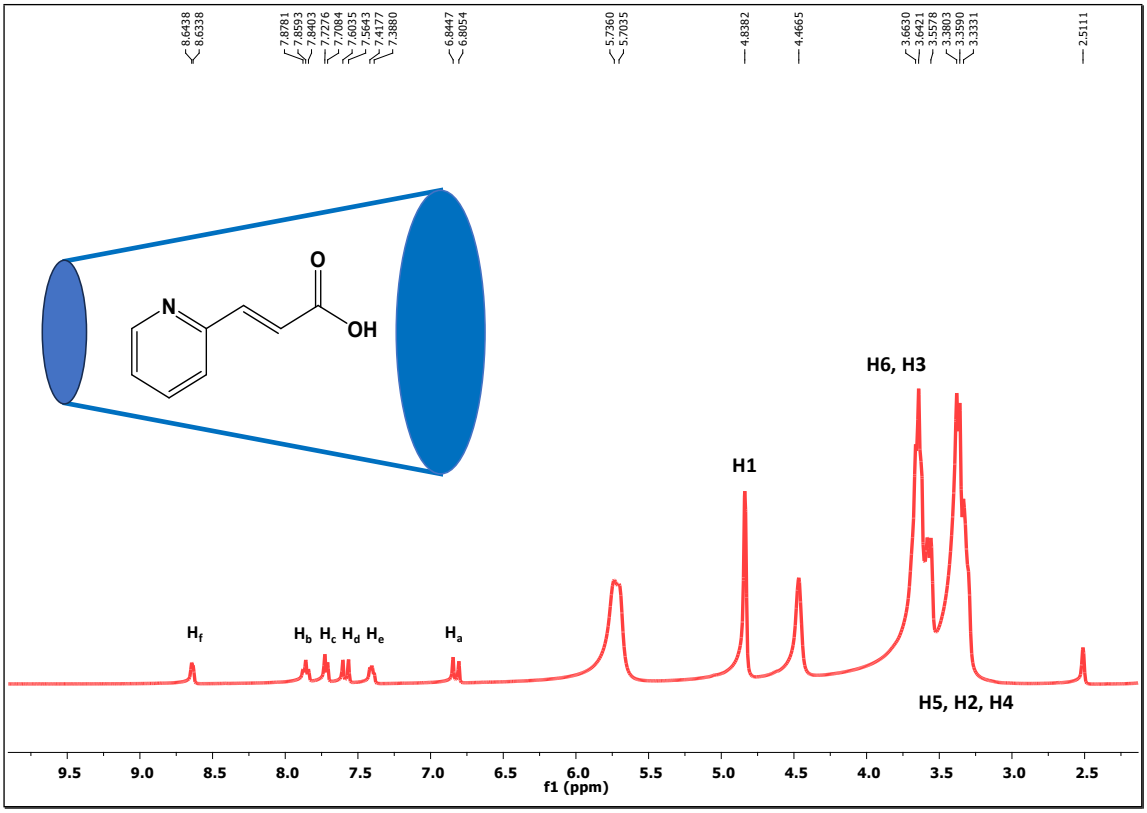

Fig.S5: ^{1}H NMR data of 3-PAA-β-CD inclusion complex.

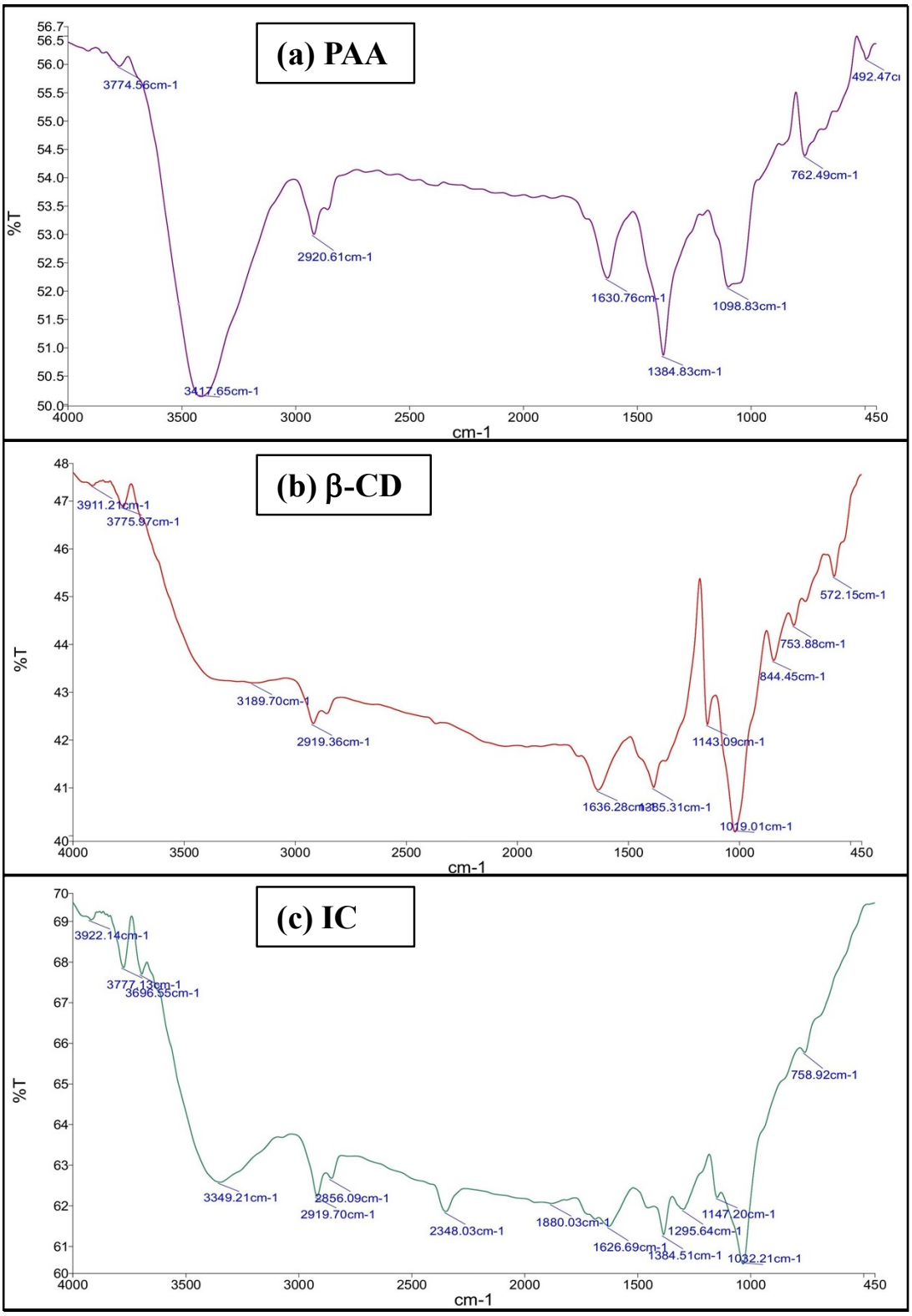

Fig.S6: FT-IR spectra of (a) 3-PAA, (b) β-CD, and (c) 3-PAA- β-CD IC

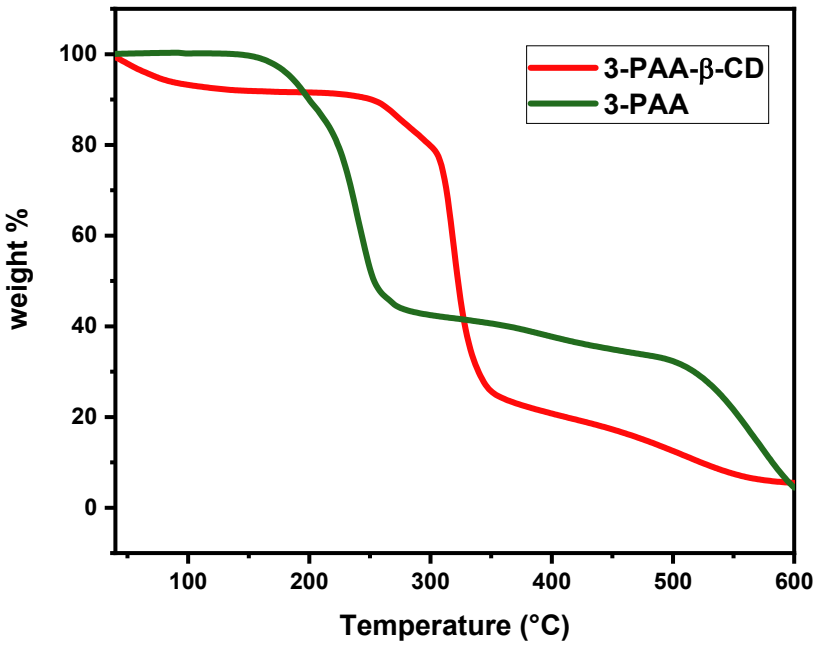

Fig.S7: TGA thermograms of pure 3-PAA, and 3-PAA-β-CD ICs.

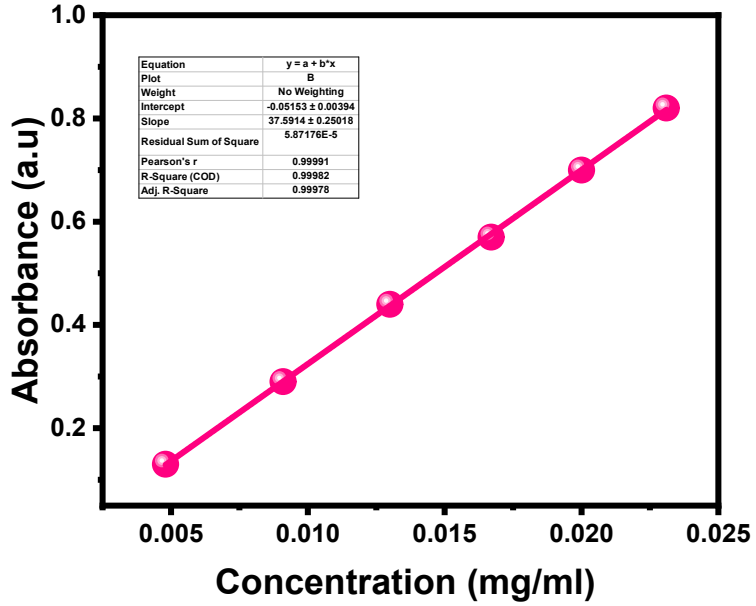

Fig.S8: UV–visible absorbance versus concentration calibration curves of free 3-PAA in aqueous medium at λmax ≈ 284 nm.

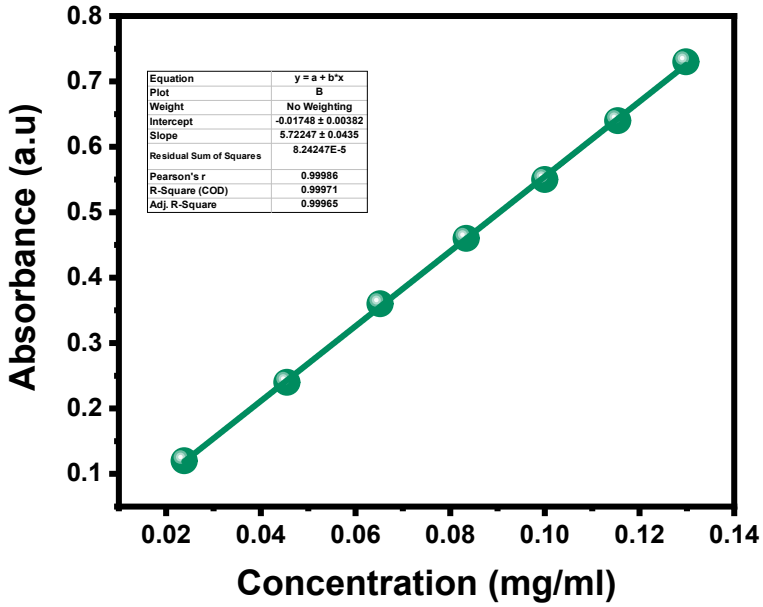

Fig.S9: UV–visible absorbance versus concentration calibration curves of 3-PAA–β-CD inclusion complex in aqueous medium at λmax ≈ 284 nm.

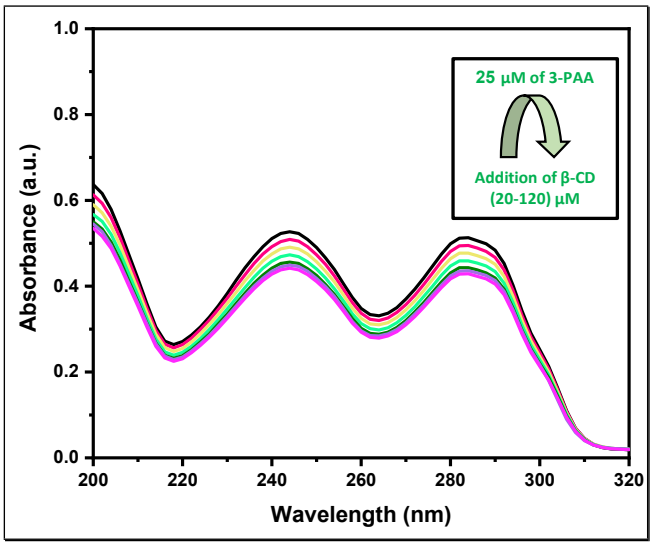

Fig.S10: Plot of Association constant (Ka) between 3-paa and IC

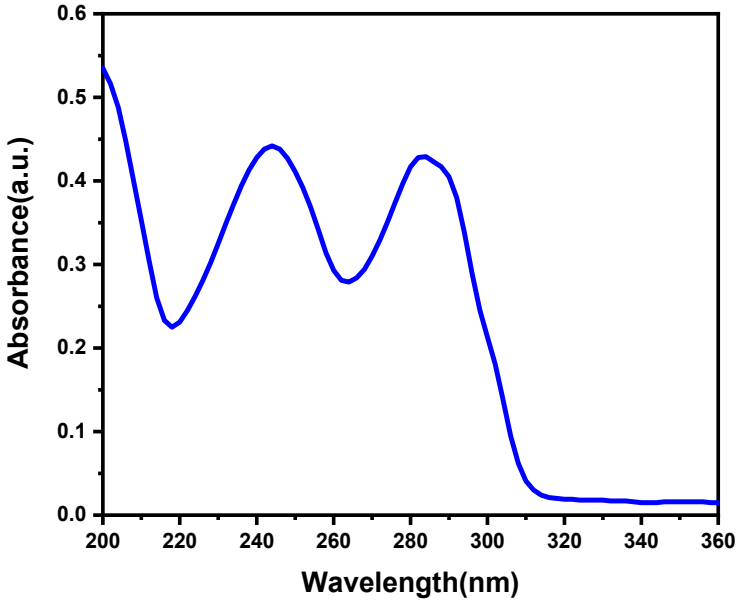

Fig.S11: UV-Vis spectra of saturated concentration of IC.

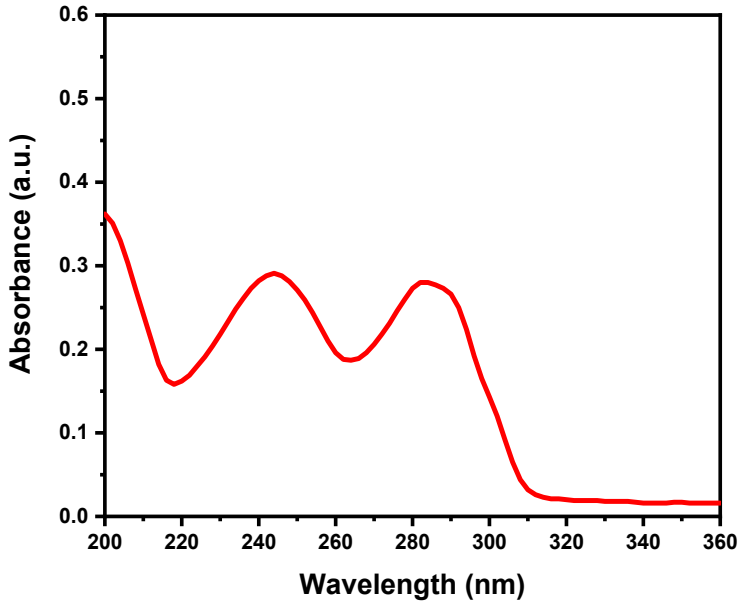

Fig.S12: UV-Vis spectra of saturated concentration of 3-PAA.

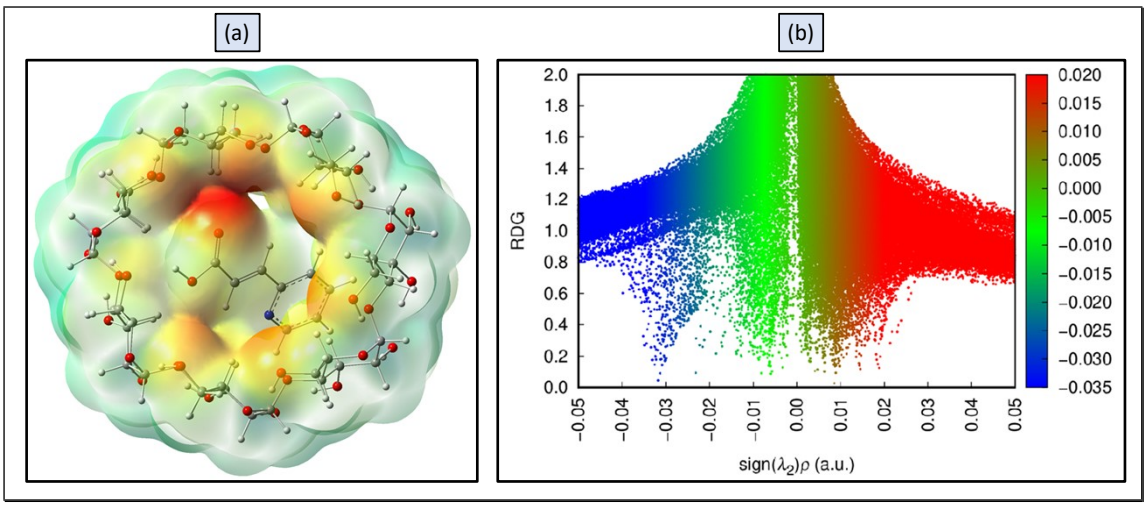

Fig.S13: (a) Electrostatic potential maps for 3-PAA-β-CD composite. (b) Plots of reduced density gradient (RDG) for 3-PAA-β-CD composite the prominent encapsulation of 3-PAA within β-CD is substantiated by all presented theoretical evidence, which corresponds effectively with the reported experimental data.

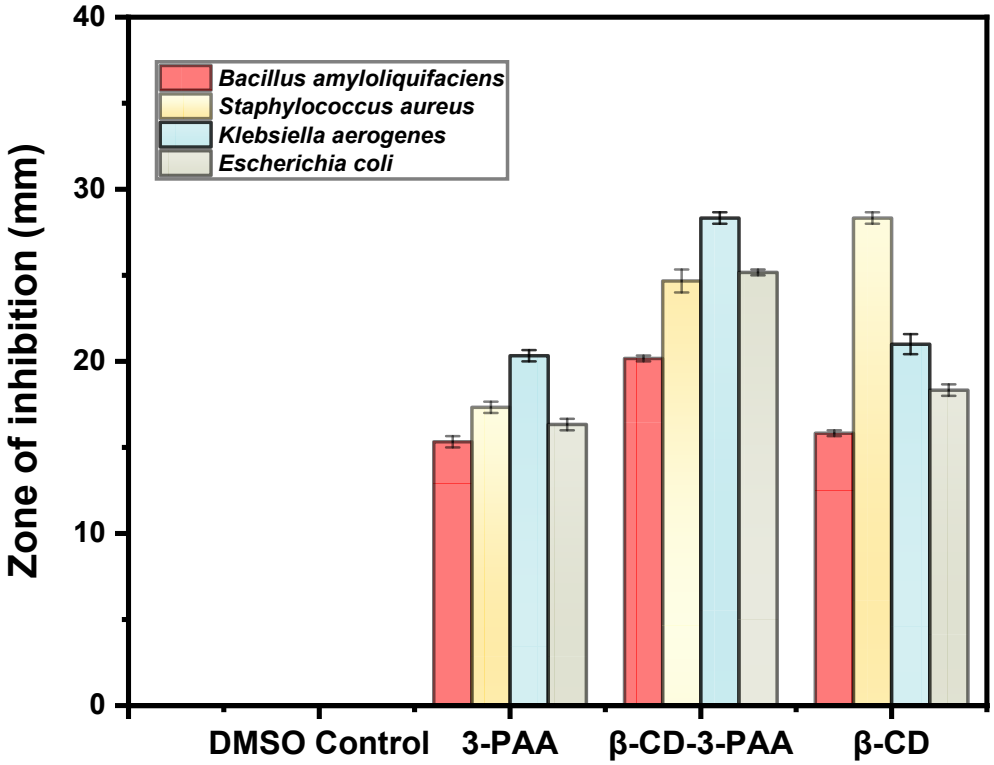

Fig.S14: Zone of inhibition (mm) analysis of 1. DMSO control, 2. 3-PAA, 3. β-CD-3-PAA, and 4. β-CD against a. Bacillus amyloliquifaciens, b. Staphylococcus aureus, c. Klebsiella aerogenes, d. Escherichia coli.

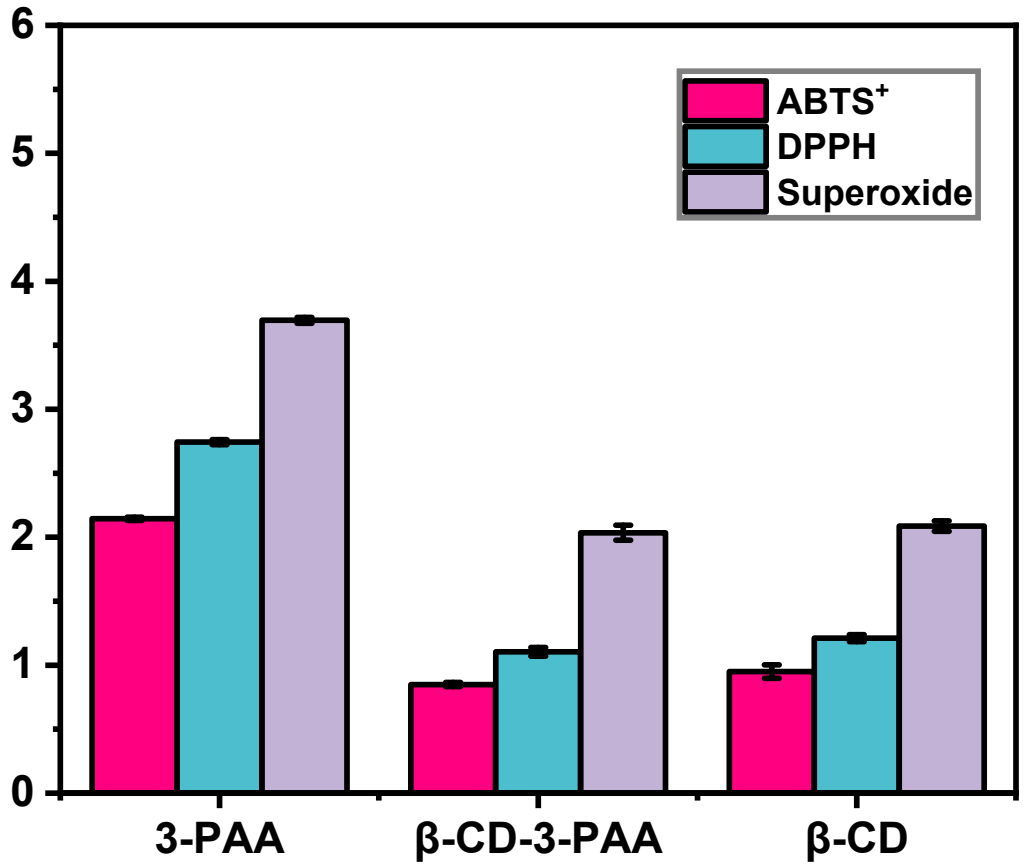

Fig.S15: Comparative antioxidant activities of 3-PAA, β-CD-3-PAA, and β-CD evaluated by ABTS•⁺, DPPH•, and superoxide (O_2•⁻) radical scavenging assays.